



Fluorescent polydopamine based molecularly imprinted sensor for ultrafast and selective detection of p-nitrophenol in drinking water

Yeqing Xu¹ · Ting Huang¹ · Minjia Meng¹ · Yongsheng Yan¹

Received: 23 August 2021 / Accepted: 8 November 2021 / Published online: 11 December 2021
© The Author(s), under exclusive licence to Springer-Verlag GmbH Austria, part of Springer Nature 2021

Abstract

A highly effective fluorescent molecularly imprinted sensor (F-PDA-MIS) based on fluorescent polydopamine (F-PDA) was successfully synthesized for selective and ultrafast detection of p-nitrophenol (P-NP) in drinking water. F-PDA with abundant surface functional groups has been artfully modified to firstly serve as both fluorescent monomer and functional monomer in the synthesis of a uniform luminous F-PDA-MIS, which can greatly improve the detection efficiency. As expected, F-PDA-MIS had an obvious emission wavelength of 535 nm with the optimal excitation wavelength at 400 nm. Specially, F-PDA-MIS could detect P-NP in the range 100 to 1100 nM with much lower detection limit of 24.2 nM within 120 s compared with other conventional imprinted fluorescent sensors based on pure quantum dots (QDs) or dyes. This excellent test phenomenon is mainly ascribed to the rapid electron transfer between F-PDA and P-NP. Satisfactory recovery of 98.0–104% for mineral water and 98.6–106% for boiling water were obtained with relative standard deviations (RSDs) of 2.7–3.4% and 2.6–3.5% respectively. The detection reliability of F-PDA-MIS was verified by the comparison with high-performance liquid chromatography (HPLC–UV). Consequently, F-PDA as a fluorescence functional monomer has been shown to be a possible strategy to effectively improve the detection limit and shorten response time of the target determination in water.

Keywords Fluorescent polydopamine · Molecularly imprinted technique · Fluorescent functional monomer · p-Nitrophenol · Rapid response

Introduction

P-nitrophenol (P-NP) is an important intermediate of chemical raw materials. It is extensively used in the manufacture of explosives, dyes, pharmaceuticals, and pesticides [1, 2]. P-NP has an accumulative effect; it can exist in water for a long time and then continuously enriched through the food chain; finally, it will attack the human immune system and cause the increasing of cancer risk [3]. Therefore, P-NP has been listed as one of

68 pollutants that need priority control in water in China [4]. The concentration of P-NP in daily drinking water is stipulated to be not higher than 0.14 μM [5]. Moreover, the maximum concentration of P-NP permitted in drinking water by the US Environmental Protection Agency is 0.43 μM [6–8]. So, it is of great importance to accurately detect P-NP in drinking water, which is closely related to human's physical health. Recently, the common analytical methods for the detection of P-NP are mainly ultraviolet spectrometry [9], electrochemical analysis [10, 11], high-performance liquid chromatography (HPLC–UV) [12], gas chromatography (GC–PID) [13], and fluorescence analysis [14–16]. Consequently, fluorescence analysis was superior to other analysis method and has been widely used in the analysis of templates due to its advantages of sensitivity and relatively low cost. However, the defects in selectivity greatly limit its scope of application; thus, constructing a fluorescence sensor with selective detection capability is of great significance.

✉ Minjia Meng
mmj@ujs.edu.cn

✉ Yongsheng Yan
yys@ujs.edu.cn

¹ Institute of Green Chemistry and Chemical Technology, Advanced Chemical Engineering Laboratory of Green Materials and Energy of Jiangsu Province, School of Chemistry and Chemical Engineering, Jiangsu University, Zhenjiang 212013, China

Molecular imprinted technology (MIT), which is a technology aimed to synthesis molecular imprinted sensors (MIS), matched with templates in size, shape, and spatial structure. Nowadays, MIT has been artfully applied to improve the selectivity for templates in fluorescence analysis [17]. Generally, the common way of building fluorescent molecularly imprinted sensor (F-MIS) is to construct a core-shell type fluorescent sensor, which used fluorescent monomer (quantum dots, organic dyes and rare earths) as the core of F-MIS, the shell layer as imprinted layer to avoid the leakage of fluorescent monomer to realize the selective detection of templates. However, it will inevitably lead to a decrease in sensitivity and a delay in detection time. Wang et al. [18] regulated the thickness of imprinted layer to improve the detection time and efficiency and finally drew a conclusion that the thinner the imprinted layer was benefit to improve the detection time and detection sensitivity. Yet the approach has some drawbacks: One is the uncontrollability of the imprinted layer and the complication of the regulatory process, and another is the damage caused by the leakage of fluorescent monomer from the thin imprinted layer. So, it is a challenge to construct an F-MIS in which synthesis and fluorescent detection performance can be well balanced.

Fluorescent polydopamine (F-PDA) is an environmental and biofriendly fluorescent organic material formed by self-polymerization of dopamine [19, 20]. Recently, F-PDA has fleetly entered into a wide range of applications, spanning the fields of energy [21], environment [22–27], biomedical [28, 29], and biosensors [30–33]. However, inspired by the multiple modifiable groups (adjacent hydroxyl, amidogen and imino groups) on the surface of F-PDA. The response time delay of common F-MIS can be effectively overcome by the usage of F-PDA as the fluorescent functional monomer. Since using F-PDA as the fluorescent functional monomer in the polymerization reaction greatly speeded up the binding time with the target, thereby increasing the response time of F-MIS to the target.

In this work, a novel F-MIS based on F-PDA (F-PDA-MIS) was successfully synthesized and applied to detect P-NP. F-PDA was prepared and optimized by reaction time and reactant concentration, etc. Moreover, F-PDA was modified by C=C to act as fluorescent functional monomer, P-NP was the template, and the F-PDA-MIS were successfully synthesized by MIT using precipitation polymerization. Herein, F-PDA was firstly used as a fluorescent functional monomer in the polymerization reaction to overcome the low fluorescence performance caused by deep embedding of fluorescent substances in normal F-MIS. It could imprint P-NP on the surface of the polymer to achieve surface imprinting in a real sense and thus increase the effective identification sites of the target and shorten the detection time of the target. The F-MISs based on CdTe QDs (CdTe QDs@MIS) and rhodamine 6G (R6G@MIS) were synthesized at the same

time to compare the detection time and detection limit with F-PDA-MIS. Finally, a series of characterization techniques were used to characterize and test F-PDA-MIS. Last but not the least, the comparison experiments between fluorescence analysis method and HPLC–UV method were conducted for the P-NP determination in real samples and obtained satisfactory results.

Experimental

Reagents and materials

P-nitrophenol (P-NP) (AR, 98%), polyethyleneimine (PEI) (99%), dopamine hydrochloride (DA) (98%), ethylene glycol dimethacrylate (EGDMA) (98%), 2,2-azobis (2-methylpropionitrile) (AIBN) (98%), methyl methacrylate (MMA) (AR, 99%), tellurium powder (~100 mesh, 99.99%), mercaptoacetic acid (AR, 90%), CdCl₂·2.5H₂O (99.99%), NaBH₄ (99%), rhodamine 6G (R6G) (AR), allyl glycidyl ether (AGE) (99%), o-nitrophenol (O-NP) (99%), m-nitrophenol (M-NP) (99%), catechol (CA) (AR, 99%), 2-aminophenol (2-AP) (98%), hydroquinone (HQ) (AR), p-cresol (P-Cr) (99%), 2,4-dichlorophenol (2,4-DP) (99%), 2,6-dichlorophenol (2,6-DP) (AR, 99%), and methanol (HPLC, 99.8%) were purchased from Aladdin Reagent Company (Shanghai, China). Ethyl alcohol (75%), acetic acid (AR, ≥ 99.5%), and methyl alcohol (AR, ≥ 99.5%) were bought from Guoyao Chemical Reagent (Shanghai, China). All chemicals were of analytical grade reagents, and the water used in the whole experiment was double distilled water (DDW).

Instrument

The model of heating magnetic stirrer is RET basic (IKA, Germany). The electronic balance model is TE124S (Sartorius, Germany). The structure and composition analysis of nanomaterial were investigated by Nicolet NEXUS-470 apparatus Fourier transform infrared (FT-IR, USA); thermal gravity analysis (TGA) was performed using Diamond TG instruments (PerkinElmer, USA). The laser confocal microscope (LCSM), TCS SP5 II was bought from brookhaven instruments companies in the United States. We measured fluorescence performance with F98 fluorescence spectrophotometer (Shanghai Leng Light Technology Co. LTD, China). The morphologies were investigated by transmission electron microscope (TEM, JEOL, JEM-2100). HPLC–UV (Agilent 1260 Infinity II) was used to detect 4-NP in actual samples.

Preparation of F-PDA

The preparation of F-PDA referred to the previous synthesis method with some modifications [34]. Firstly, compounded a

series of different concentrations of PEI solution with DDW. Next, a series of different concentrations of dopamine solutions were prepared and added into the PEI solution, respectively, and stood for a period of time to wait for the color of solutions turning into bistre and then stirred in DDW with a 3500 Da dialysis bag for 24 h to filter out unreacted reactants and impurities to obtain pure fluorescent polydopamine. Finally, all the solutions were freeze dried under $-90\text{ }^{\circ}\text{C}$ and were stored in $4.0\text{ }^{\circ}\text{C}$ for further use.

Preparation of fluorescence functional monomer (F-PDA-AGE)

To use the F-PDA as a fluorescence functional monomer, C=C unsaturated double bond is essential to provide the possibility of imprinting polymerization. In this work, the F-PDA-AGE was synthesized according to the previous method with some modifications [35]. Briefly, the dialyzed F-PDA and AGE ($v:v = 1.0: 1.1$) were dissolved in ethanol to control the total concentration of reactants at 0.2 g/mL . The reaction was refluxed at $75\text{ }^{\circ}\text{C}$ for 12 h under nitrogen atmosphere. Then, the solvent ethanol in the system was distilled off under reduced pressure at $60\text{ }^{\circ}\text{C}$ and, finally, precipitated in n-hexane, treated for three times, and freeze dried under $-90\text{ }^{\circ}\text{C}$ to obtain a high-viscosity product F-PDA-AGE.

Preparation of F-PDA-MIS

The synthesized F-PDA-AGE was well water-soluble but slightly soluble in ethanol and meanwhile insoluble in acetonitrile, so ethanol was selected to be the reaction medium. The first step was the preparation of precursor solution; P-NP and EGDMA were added in 20 mL ethanol with a certain mole ratio ($n_{\text{P-NP}}:n_{\text{EGDMA}} = 1:16$). After dispersing evenly with ultrasonic machine, it was allowed to stand for 2.0 h. Secondly, 1.0 mL F-PDA-AGE was dissolved in 5.0 mL DDW primarily; 35 mL ethanol was added subsequently. In the third step, the aforesaid two solutions were mixed uniformly and stood for 30 min with nitrogen; next, a certain amount of initiator (AIBN) was added to induce the reaction under $60\text{ }^{\circ}\text{C}$ stirring for 24 h. The last step was the elution of P-NP; the F-PDA-MIS were collected by centrifugation and washed repeatedly with ethanol and DDW. After that, F-PDA-MIS was eluted with 100 mL of acetic acid/methanol (1:9, v/v) to dislodge P-NP by Soxhlet extractor for 3.0 d and then collected again and dried at $40\text{ }^{\circ}\text{C}$ under vacuum overnight.

The synthetic processes of fluorescent non-imprinted polymer (F-PDA-NIS) were similar with F-PDA-MIS except the addition of P-NP. Another NIS without F-PDA and P-NP (N-NIS) were synthesized by precipitation polymerization which used MMA as a functional monomer ($n_{\text{P-NP}}:n_{\text{MMA}}:n_{\text{EGDMA}} = 1:4:16$). The CdTe QDs@MIS and R6G@MIS were synthesized by the same method with

F-PDA-MIS except for the addition of fluorescent materials. Specially, the addition of CdTe QDs and R6G were all of 1.0 mL, respectively.

Fluorescence detection of P-NP

In order to apply F-PDA-MIS into actual environment, a series of questions would be considered, such as the stability of F-PDA-MIS, reaction time for targets, pH of detection environment, identification of similar substances, and inference of co-existing ions. First, F-PDA-MIS (about 0.4 g/L) were dispersed in colorimetric tubes evenly as a stock solution; then the stock solution ($500\text{ }\mu\text{L}$) was dissolved in 5.0 mL DDW as the test solution; P-NP solutions with a certain concentration gradient were added to the test solution to perform fluorescence detection; and a linear relationship equation between fluorescence intensity and target concentration was obtained. In selective studies, O-NP, M-NP, CA, 2, 6-DP, 2-AP, HQ, P-Cr and 2, 4-DP were selected to explore the specificity of F-PDA-MIS to P-NP, finally was the inference of co-existing ions in surrounding environment. All the fluorescence detections above were tested under room temperature by a F98 fluorescence spectrophotometer, the excitation wavelength was set at 400 nm, the slit width of emission and excitation was both set at 10 nm, and finally, the energy of the photomultiplier tube was set to 800 V. Similar tests were compared under the same testing conditions.

HPLC–UV analysis of actual samples

The HPLC–UV analysis method was referred to “Urine-Determination of p-nitrophenol-High-performance liquid chromatographic method (WS/T 58–1996),” which was issued by the Ministry of Health of the People’s Republic of China. Specially, a HPLC–UV (Agilent 1260 Infinity II) with Wonda Cract ODS-2 reversed-phase column ($250\text{ mm} \times 4.6\text{ mm}$, $5\text{ }\mu\text{m}$) was used for chromatographic separation at the $55\text{ }^{\circ}\text{C}$ column temperature. The mobile phase was an isocratic eluent of the mixture of methanol and purified water ($v:v = 30\%:70\%$) under a 317 nm UV detector. The flow rate was set at $1.0\text{ mL}\cdot\text{min}^{-1}$, and the injected volume of samples was $5.0\text{ }\mu\text{L}$ with a detection time of 30 min.

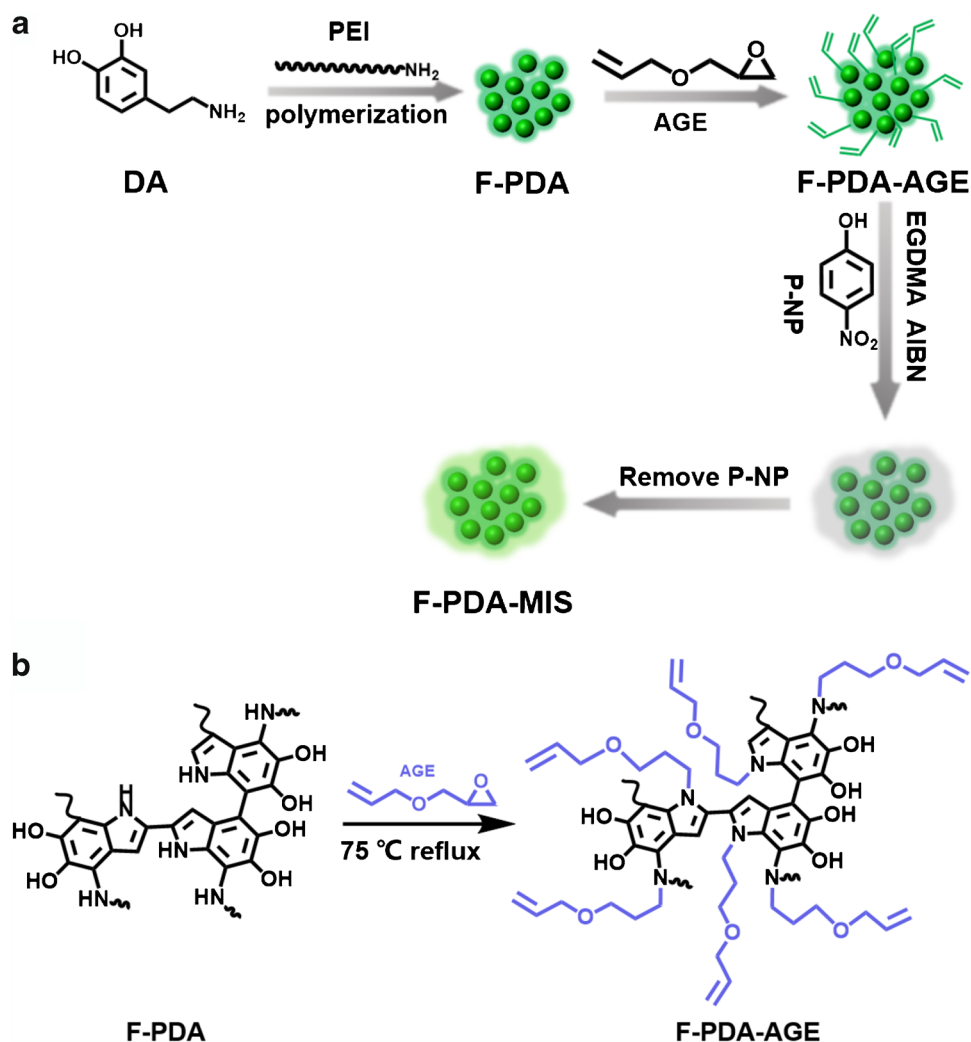
The actual samples of the mineral water and the boiling water were firstly filtered for three times through the water-phase filter membrane to remove the macromolecular impurities. Finally, the actual samples were sampling and testing by HPLC–UV analysis.

Results and discussion

Synthesis and characterization of F-PDA-MIS

Scheme 1a is the prepared scheme of F-PDA-MIS; as could be seen in the picture, the F-PDA was synthesized

Scheme 1. **a** Synthesized process of F-PDA-MIS; **b** C=C modification of F-PDA



by oxidation of dopamine in an alkaline environment; the green fluorescence F-PDA was obtained after dialysis purification. For the diversity of surface functional groups of F-PDA, F-PDA was connected to the double key and provided the possibility of imprinting polymerization (Scheme 1b). Therefore, in this study, F-PDA played the roles of both fluorescent material and functional monomer in polymerization reaction; P-NP was the target analysis and had great electrical absorption, which could pull the electrons that transition to the excited state in F-PDA to their own groups, thereby reducing the probability of electronic transitions from the excited state to the ground state, resulting in the fluorescence quenching of F-PDA. EGDMA was used as a cross-link; F-PDA-MIS were synthesized by precipitation polymerization, which were used for the detection of P-NP.

Figure 1a and b are the TEM images of F-PDA and F-PDA-MIS; as shown in the pictures, F-PDA was tiny, and the size was on the quantum scale, in which the diameter was about 2.0 nm. Figure 1b is the TEM image of F-PDA-MIS.

It could be seen from the figure that the F-PDA formed the polymer with irregular shape after the polymerization reaction, but the polymer did not produce the double agglomeration phenomenon, and the dispersion was good. Figure 1c is the laser scanning confocal microscope (LSCM) images of F-PDA-MIS, in which excitation wavelength was 365 nm; as the picture shown, the entire surface of the F-PDA-MIS glowed bright fluorescence and distributed very evenly; this indicated that F-PDA participated in the reaction as a substitute of functional monomer, not just a fluorescent material. In other words, F-PDA directly participated in the reaction and maintained its fluorescent properties. It was evenly dispersed on the surface of F-PDA-MIS to form a homogeneous and stable fluorescent imprinted polymer. Next, Fig. 1d and e are the pictures of F-PDA-MIS and N-NIS under daylight and 365 nm UV lamp, respectively; compared to F-PDA-MIS with N-NIS, the color of F-PDA-MIS under daylight was light brown, while N-NIS was white, and the color of F-PDA-MIS under 365 nm was bright green, while N-NIS had no color.

Mechanism 1 Diagram of the recognition mechanism of F-PDA-MIS and P-NP

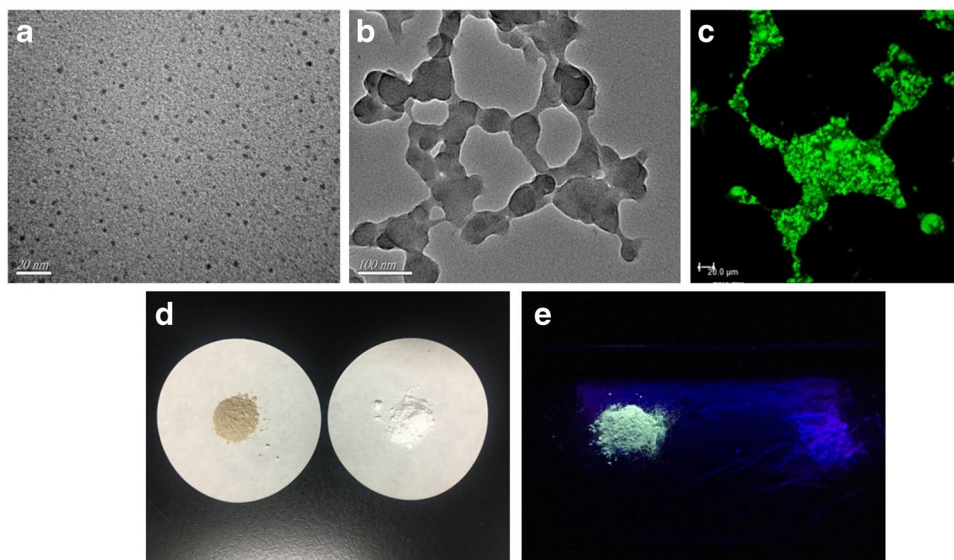
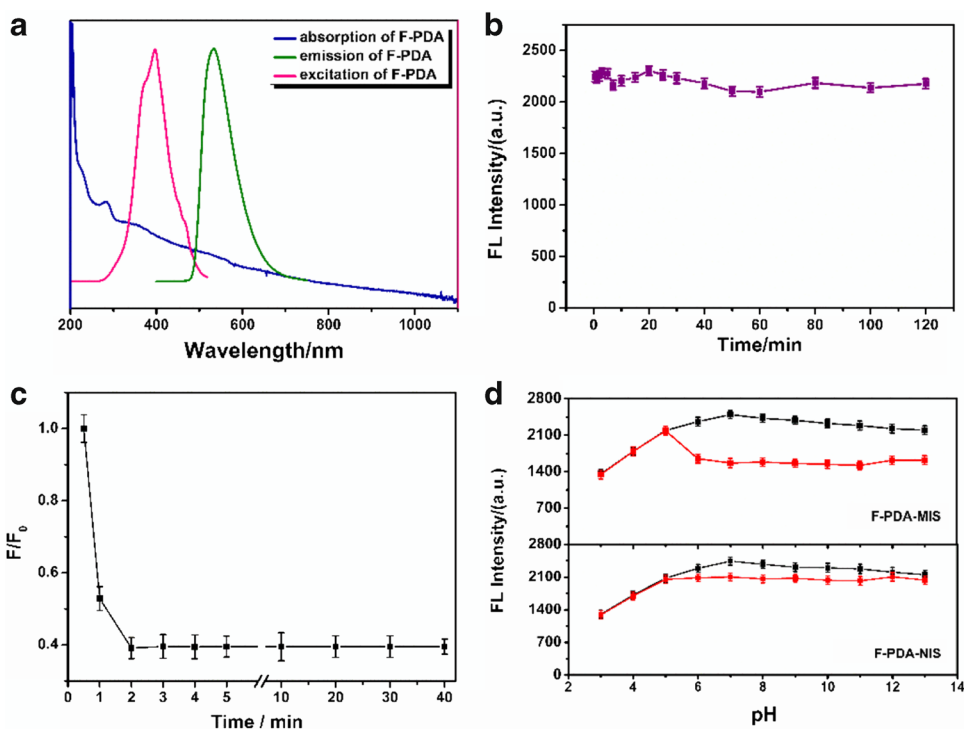


Fig. 1 TEM images of F-PDA (a) and F-PDA-MIS (b); LSCM image of F-PDA-MIS (c); pictures of F-PDAMIS (left) and N-NIS (right) under daylight (d) and 365 nm UV lamp (e)



There have been many functional groups on the surface of F-PDA, but there were no carbonized double bonds, and molecularly imprinted polymerization could not be carried out on the surface of F-PDA to improve the selectivity when recognizing the targets. Therefore, double-bond end capping was conducted to synthesize F-PDA with C=C. Figure S5a is the ¹HNMR spectra of F-PDA and F-PDA-AGE; compared to F-PDA with F-PDA-AGE, it could be observed that there were obviously C=C characteristic peaks between 5.0 and 6.0 ppm, which indicated that C=C was successfully

modified on the surface of F-PDA. FT-IR spectra of F-PDA, F-PDA-AGE, and F-PDA-MIS are shown in Figure S5b; the three materials had a distinct characteristic peak around 3300 cm⁻¹, which was the stretching vibration peak of -OH on F-PDA. Next, the F-PDA was contacted with AGE; the peak at 1109 cm⁻¹ was the stretching vibration peak of the ether bond, which indicated that AGE was successfully connected to the surface of F-PDA. Finally, F-PDA was involved in the polymerization reaction to form the F-PDA-MIS; several small peaks appeared in the infrared spectra

of F-PDA-MIS; the peak at 1160 cm^{-1} was a stretching vibration peak of the ether bond; the peak at 1257 cm^{-1} was the bending vibration peak of $-\text{CH}_3$, at 1388 cm^{-1} was the stretching vibration peak of C-O, and at 1728 cm^{-1} was the stretching vibration peak of C=O; these new characteristic peaks were functional groups of EGDMA, which indicated that the F-PDA-MIS were synthesized successfully. Figure S6 is the thermogravimetric analysis (TGA) data of F-PDA-MIS and F-PDA-NIS; as shown in the picture, the initial thermal weight loss is due to the internal crystal water disappearing with the increase of temperature; when the temperature rose to 270–430 °C, the crosslinking agent and functional monomers gradually decomposed as the temperature rose; finally, the weight loss of F-PDA-MIS and F-PDA-NIS were 6.91% and 6.44% respectively. The above analysis results well illustrate that a polymer layer successfully coated on the surface of F-PDA and the polymers had good thermal stability.

Fluorescence quenching mechanism

As shown in Mechanism 1, F-PDA is formed by the oxidative polymerization of dopamine in an alkaline environment containing PEI. There were many functional groups on the ring of F-PDA, such as $-\text{OH}$, $-\text{NH}_2$, and $-\text{NHR}$, which were all electron-donating functional groups, so the excited state of F-PDA is usually excited by the n electrons on the hydroxyl and amino outside the ring and transferred to the ring to produce fluorescence. In order to further explore the quenching mechanism of P-NP quenching fluorescence of F-PDA. The transient fluorescence lifetime diagrams of F-PDA and the mixture of F-PDA and P-NP were exhibited in Figure S7a and Figure S7b, respectively. The first-order fitting was selected as the best fit formula by the comparisons of second-order fitting and third-order fitting [36, 37], finally, the τ and τ were calculated to 4.19 ns and 3.21 ns respectively, $\tau/\tau \neq 1$, this result indicated that the quenching mechanism couldn't be static quenching. Next, the UV–vis absorption spectra of P-NP and F-PDA and the mixture of F-PDA with P-NP were measured, as displayed in Figure S7c; the ultraviolet absorption peak of F-PDA did not shift significantly after adding P-NP, which indicated that there was no complex formed between F-PDA and P-NP; therefore, the possibility of internal filtration effect (IFE) [38] was ruled out. However, the position of the emission peak of F-PDA and the ultraviolet absorption peak of P-NP was quite different, so it was impossible for them to be fluorescence quenching caused by fluorescence resonance energy transfer (FRET) [39]. Finally, zeta potentials of F-PDA and P-NP and mixture of F-PDA and P-NP under the same test pH conditions were tested, and the results in Figure S7d demonstrated that there had been electrostatic attraction between F-PDA and P-NP. Thence, electron

transfer (ET) [1] was the dominating quenching mechanism in this sensor, and the quenching mechanism is showed in Mechanism 1 detailly.

Optimization of detection conditions

Before detecting P-NP, the detection conditions should be explored. Firstly, the fluorescence dependence of F-PDA was conducted to select the optimal excitation wavelength. Figure 2a is the absorption spectrum, fluorescence emission spectrum, and fluorescence excitation spectrum of F-PDA; it could be found that the absorption peak of F-PDA was at 280 nm, the emission wavelength of F-PDA was as 535 nm, and the optimal excitation wavelength of F-PDA was at 400 nm (Fig. 2a). Next was the stability of F-PDA-MIS, the FL intensities of F-PDA-MIS were detected for many times in 2.0 h, the results are displayed in Fig. 2b, and the results were clear that the FL intensities of F-PDA-MIS fluctuated only slightly within 2.0 h. Therefore, F-PDA-MIS could remain relatively stable within 2.0 h, meeting our experimental detection requirements.

Figure 2c is the reaction time of F-PDA-MIS when a certain amount of P-NP were added into the F-PDA-MIS solution; specifically, 500 μL of stock solution was dissolved in 5.0 mL DDW as the blank detection solution; a certain amount of P-NP (100–1100 nM) were added into the blank detection solution; the FL intensities were detected when P-NP was added to the detection solution; and the fluorescence intensities of F-PDA-MIS at different times after the addition of P-NP were recorded until its fluorescence intensity was relatively stable. The corresponding result is shown in Fig. 2c; the response time of F-PDA-MIS to P-NP was 2.0 min, which was faster than the reaction time of general polymers. Therefore, using F-PDA as a substitute of traditional functional monomer could better achieve the surface imprint of the target and improve its response time to the target.

Figure 2d is the inference of pH value on the detection of F-PDA-MIS; the FL intensities of F-PDA-MIS and F-PDA-NIS before (black line) and after (red line) the addition of 400 nM P-NP under different pH value ranging from 3.0 to 13.0 were detected under the same test conditions. It could be seen from the test results that F-PDA-MIS and F-PDA-NIS had strong fluorescence intensity in a neutral environment and relatively weak fluorescence intensity in an over-acidic or over-alkaline environment. When the pH was around 7.0–9.0, the F-PDA-MIS and F-PDA-NIS had the best recognition effect on P-NP. Therefore, this experiment was more suitable to be performed in a pH around 7.0–9.0.

Fluorescent detection of P-NP

The detective capability of F-PDA-MIS was the final purpose of the research, so the F-PDA-MIS were dissolved in

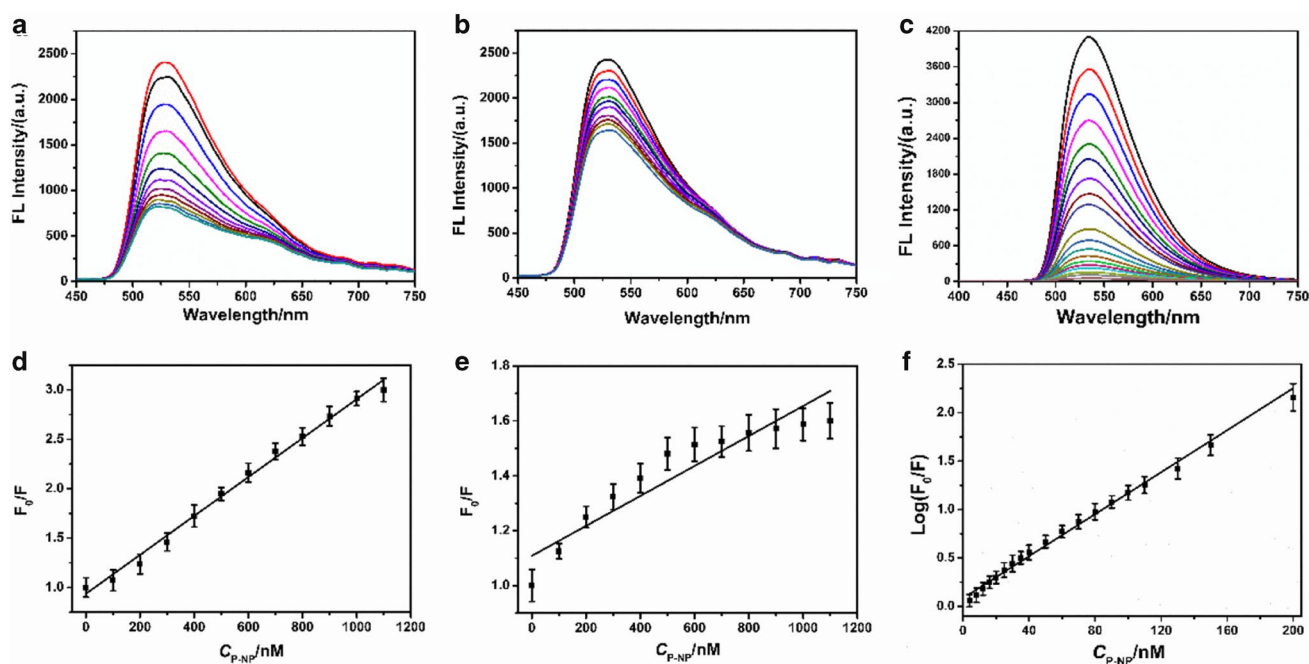


Fig. 2 **a** Absorption spectrum (blue line), fluorescence emission spectrum (green line), and fluorescence excitation spectrum (pink line) of F-PDA; **b** fluorescent intensities of F-PDA-MIS in 120 min; **c** fluorescent intensity of F-PDA-MIS in the presence of 800 nM P-NP at

different incubation time; **d** effect of pH on fluorescence intensity of F-PDA-MIS and F-PDA-NIS before (black line) and after (red line) addition of 400 nM P-NP

DDW to be the stock solution and waited for the detection of P-NP, first of all, F-PDA-MIS were dissolved again in a colorimetric tube as a blank control, the target P-NP of different concentrations were added into blank solutions, and the FL intensity of blank control and solutions with P-NP were recorded, as shown in Fig. 3a, with the increasing concentration of P-NP ranged from 100 to 1100 nM, the FL intensity of F-PDA-MIS was decreased in turn, linear relationship between FL intensity ratio and concentrations of P-NP (C_{P-NP}) was gained by calculating F/F_0 , which F_0 represented the FL intensity of blank control, F represented FL intensity of solutions with P-NP, linear relation was $F/F_0 = 0.00199C_{P-NP} + 0.92566$, and linearly dependent coefficient (R^2) was 0.99304. It could be seen from the results that the F-PDA-MIS synthesized in this experiment had a good linear relationship with the concentration of P-NP and could be used to detect the concentration of P-NP in actual samples. Finally, limit of detection (LOD) was calculated by formula: $LOD = 3\sigma/k$ ($n = 10$), where σ indicated as the relative standard deviation (RSD) after blank control was tested for 10 times, k expressed as the slope of a linear curve, and n was the testing times. The LOD is calculated to 24.2 nM [16].

To explore the sensitivity of F-PDA-MIS, the fluorescent changes of F-PDA-NIS with P-NP were detected at the same time under the same test conditions; as could be seen in Fig. 3b, the FL intensities of F-PDA-NIS

could decrease gradually with the addition of P-NP, but it was not a significant drop compared with F-PDA-MIS; the linear regression equation of F-PDA-NIS was $F/F_0 = 0.00041849C_{P-NP} + 1.01556$; linearly dependent coefficient (R^2) was 0.99348. The imprinting factor (IF) ($IF = k_{MIP} / k_{NIP}$) [40] was calculated to 4.76, which was high than 3.8 for F-PDA-MIS. The quenching rate of F-PDA-MIS and F-PDA-NIS were calculated to 64.0% and 32.3%, respectively; the quenching rate of F-PDA-MIS was twice as much as that of F-PDA-NIS. The linear equations of both F-PDA-MIS and F-PDA-NIS are displayed in Fig. 3d and Fig. 3e; as shown in the comparison of two curves, F-PDA-MIS had higher linear scope than that of F-PDA-NIS; this indicated that the concentration of P-NP had a deeper efficiency of F-PDA-MIS, which compared with F-PDA-NIS. From the above, F-PDA-MIS had good linear relationship with P-NP under the range of 100–1100 nM, which could be applied to the detection of P-NP.

In addition, the detective capability of F-PDA was explored as well; Fig. 3c displayed the FL intensity changes of F-PDA in the presence of 4.0–200 nM P-NP, the FL intensity decreased quickly with the addition of P-NP, and consequently the concentration of P-NP had a good linear relationship with $\text{Log}(F_0/F)$. As displayed in Fig. 3f, the linear regression equation of F-PDA to P-NP was $\text{Log}(F_0/F) = 2.225 \times 10^{-4} C_{P-NP} + 0.08572$, R^2 was 0.99246, the LOD of F-PDA to P-NP was calculated to 2.34 nM.

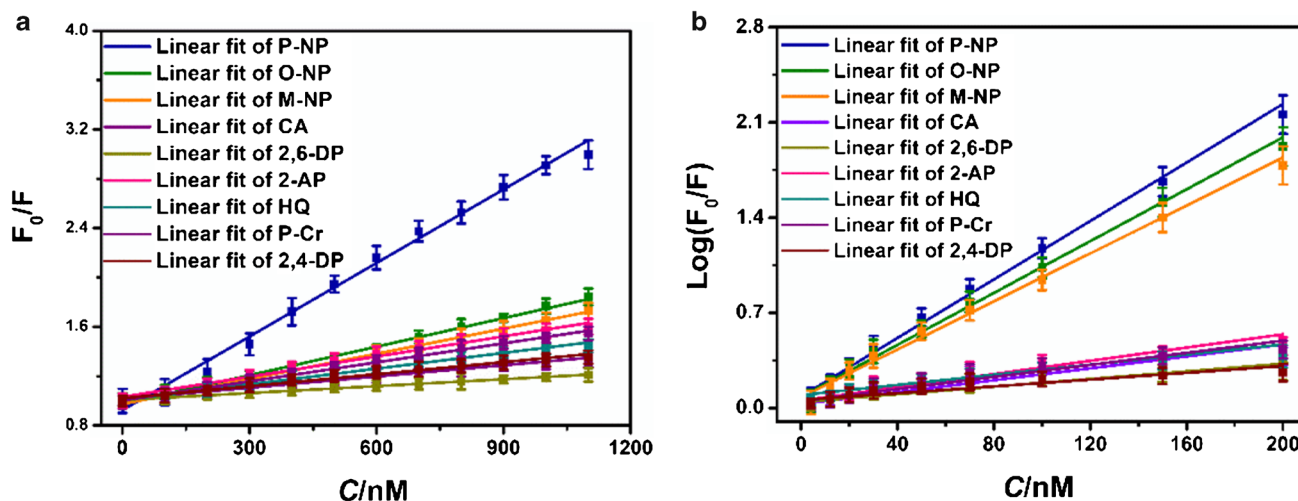


Fig. 3 Fluorescence spectra of F-PDA-MIS (a) and F-PDA-NIS (b) upon the exposure to different concentrations of P-NP range from 0 to 1100 nM; fluorescence spectra of F-PDA (c) upon the exposure to

different concentrations of P-NP range from 0 to 200 nM; linear relationship of F-PDA-MIS (d), F-PDA-NIS (e), and F-PDA (f) upon the same concentrations range of P-NP

Compared with F-PDA-MIS, F-PDA detection of P-NP did have a lower detection limit and faster detection speed, but it lacked selectivity, because F-PDA had almost the same detection ability for M-NP and O-NP as it detected P-NP.

Selective study of F-PDA-MIS

Selectivity of F-PDA-MIS was the key factor in the practical applications; it could test the responsiveness of similar substances to F-PDA-MIS, thereby judging the practicality of F-PDA@MIS. In this study, eight similar substances, O-NP, M-NP, CA, 2,6-DP, 2-AP, HQ, P-Cr, and 2,4-DP were selected to detect the responsiveness to F-PDA-MIS; for the comparison, the recognition effect of F-PDA on these targets was explored at the same time. Figure 4a showed the linear regression curves of F-PDA upon the exposure to same concentrations (4.0 to 200 nM) of P-NP, O-NP, M-NP, CA, 2,6-DP, 2-AP, HQ, P-Cr, and 2,4-DP. It could be found from the picture that P-NP, O-NP, and M-NP had a more obvious recognition effect on F-PDA than other analogs based on their strong electron-attracting effect, but the individual F-PDA could not distinguish P-NP, O-NP, and M-NP well, which indicated that the F-PDA had no selective recognition capability among P-NP, O-NP, and M-NP. Figure 4b is the linear regression equations of F-PDA upon the exposure to same concentrations (100 to 1100 nM) of P-NP, O-NP, M-NP, CA, 2,6-DP, 2-AP, HQ, P-Cr, and 2,4-DP. From the five curves, the scope of linear fit of P-NP was much higher than the others, which indicated that P-NP had greater influence on F-PDA-MIS than other substances that included O-NP and M-NP. This could be attributed to the special imprinting holes on the surface of F-PDA-MIS, which endowed F-PDA-MIS the ability to identify P-NP selectively.

Ions interference experiment

For better usage of F-PDA-MIS, it was also necessary to eliminate the interference of coexisting ions in the detection environment, so in order to detect P-NP in drinking water, the coexisting ions in drinking water included Pb^{2+} , Zn^{2+} , Cd^{2+} , K^+ , Mg^{2+} , Na^+ , Ni^{2+} , Ba^{2+} , Cu^{2+} , Li^+ , Ca^{2+} , Al^{3+} , Co^{2+} , and Fe^{3+} , which were selected to study the effect on F-PDA-MIS. Figure 5 showed the FL intensity changes of F-PDA (a) and F-PDA-MIS (b) after adding 400 μM Pb^{2+} , Zn^{2+} , Cd^{2+} , K^+ , Mg^{2+} , Na^+ , Ni^{2+} , Ba^{2+} , Cu^{2+} , Li^+ , Ca^{2+} , Al^{3+} , Co^{2+} , and Fe^{3+} respectively. The results showed that Pb^{2+} , Ni^{2+} , Cu^{2+} , Al^{3+} , Co^{2+} , and Fe^{3+} had more obvious effects on the detection of F-PDA than F-PDA-MIS, which indicated that the imprinting layer could improve the anti-interference ability of the sensor to a certain extent. After continuing to add a certain concentration of P-NP, both F-PDA and F-PDA-MIS showed an excellent recognition effect on the detection of P-NP. In other words, F-PDA-MIS could be used to detect P-NP in drinking water without disturbance.

Comparison of response time and LOD

The contrast experiments of CdTe QDs@MIS and R6G@MIS were synthesized through the same method to detect the concentration of P-NP. The fluorescent changes of CdTe QDs@MIS and R6G@MIS with P-NP concentration are showed in Fig. 6a and d; the corresponding linear relationship equations are displayed in Fig. 6b and e respectively; it could be found in the pictures that the FL intensities CdTe QDs@MIS and R6G@MIS decreased gradually with the addition of P-NP. Compared with F-PDA-MIS, the decline

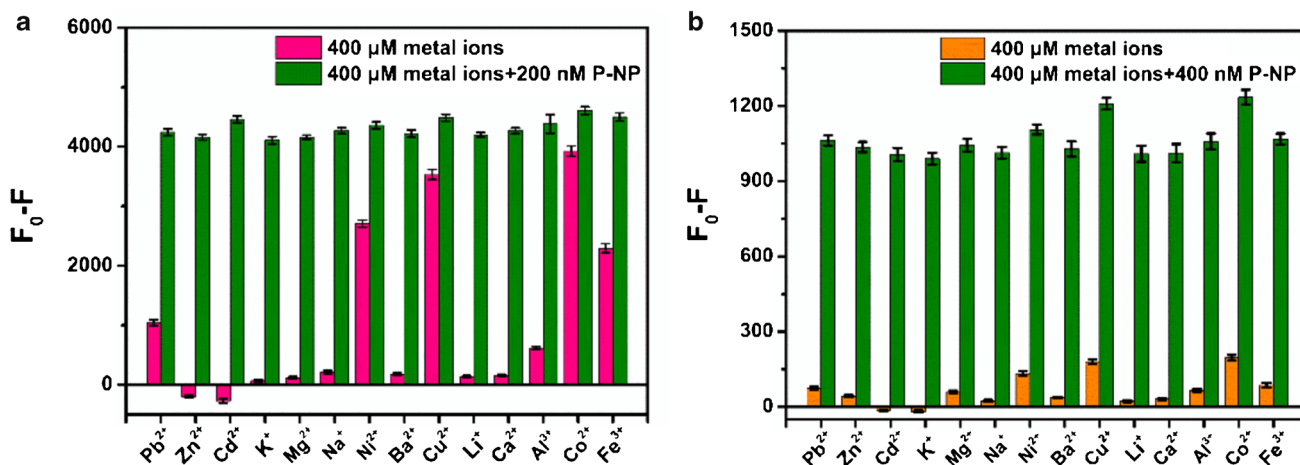


Fig. 4 Linear relationship of F-PDA (a) and F-PDA-MIS (b) upon the exposure to same concentration range of P-NP (blue line), O-NP (olive line), M-NP (orange line), CA (violet line), 2,6-DP (dark yellow

low line), 2-AP (pink line), HQ (dark cyan line), P-Cr (purple line), and 2,4-DP (wine line)

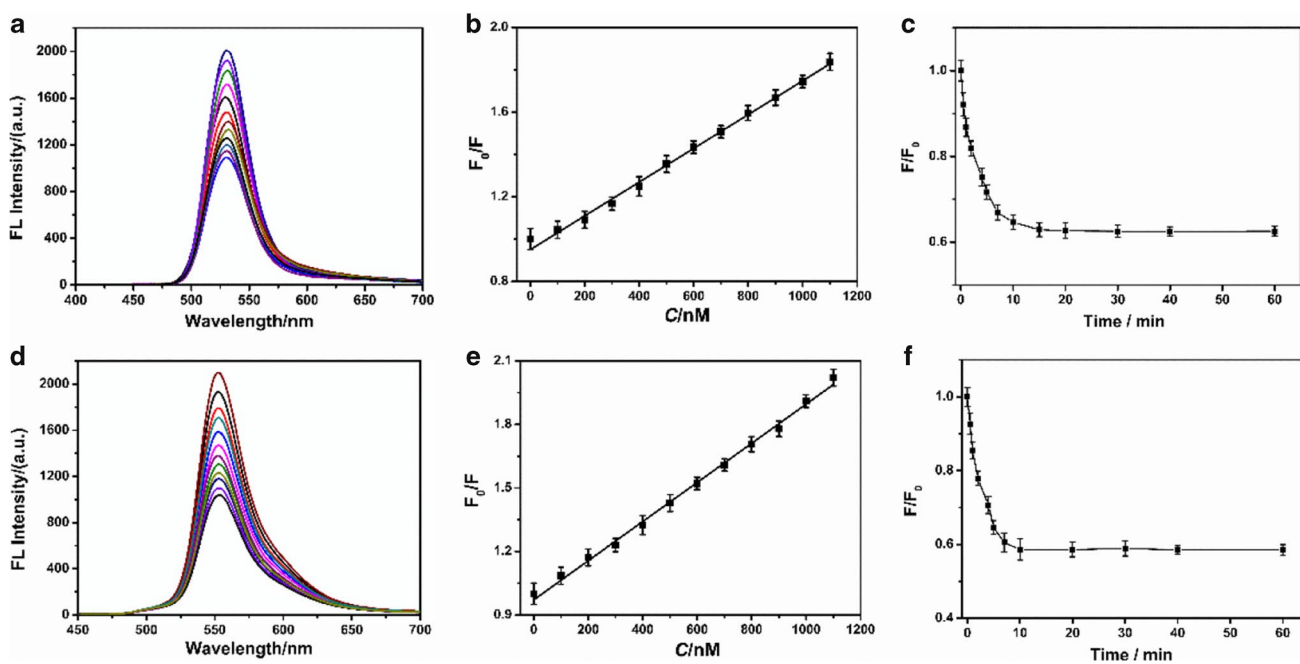


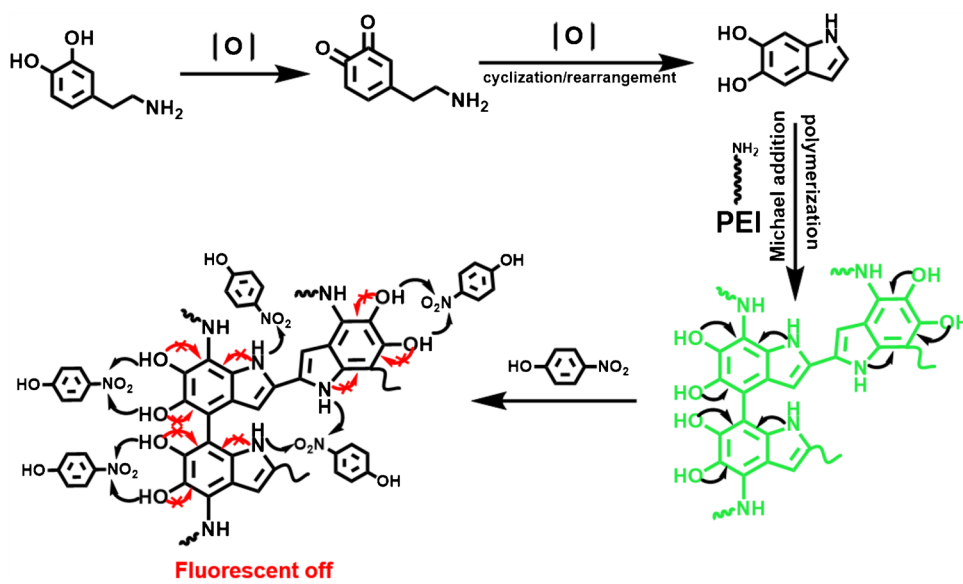
Fig. 5 Fluorescence intensity discrepancy (F_0-F) of F-PDA (a, pink bar) and F-PDA-MIS (b, orange bar) at 400 μM Pb^{2+} , Zn^{2+} , Cd^{2+} , K^+ , Mg^{2+} , Na^+ , Ni^{2+} , Ba^{2+} , Cu^{2+} , Li^+ , Ca^{2+} , Al^{3+} , Co^{2+} , and Fe^{3+} and at the presence of the mixture of metal ions and P-NP (green bar)

of the other two sensors was less obvious than F-PDA-MIS; consequently, the LOD of the two sensors was higher than which of F-PDA-MIS. Specifically, the linear regression equation of CdTe QDs@MIS was $\text{Log}(F_0/F) = 7.9723 \times 10^{-4} C_{\text{P-NP}} + 0.95034$ ($R^2 = 0.99601$), the LOD of CdTe QDs@MIS to P-NP was calculated to be 60.5 nM, the linear regression equation of R6G@MIS was $\text{Log}(F_0/F) = 9.2425 \times 10^{-4} C_{\text{P-NP}} + 0.9715$ ($R^2 = 0.9963$), the LOD of R6G@MIS to P-NP was calculated to be 52.2 nM. The LODs of CdTe QDs@MIS and R6G@MIS were both higher than

F-PDA-MIS, which may be attributed to the deep coating of fluorescent materials. Furthermore, the response time of CdTe QDs@MIS and R6G@MIS were detected and showed in Fig. 6c and f; compared with F-PDA-MIS, the response time of CdTe QDs@MIS and R6G@MIS was much longer than F-PDA-MIS. The results proved that the F-PDA as a role of fluorescent functional monomer could immensely promote the response time and detection limit.

In another hand, a series of MISs were listed to compare the detection limit and detection time together. The response

Fig. 6 Fluorescence spectra of CdTe QDs@MIS (a) and R6G@MIS (d) upon the exposure to different concentrations of P-NP range from 0 to 1100 nM. The linear relationship of CdTe QDs@MIS (b) and R6G@MIS (e). Fluorescent intensity of CdTe QDs@MIS (c) and R6G@MIS (f) in the presence of 800 nM P-NP at different incubation times



time of various MISs is shown in the Table S1; the types of MISs, their corresponding analysis targets, linear ranges, and detection limits were also listed in the following table. Especially, compared to this work to the last work listed in Table S1, the response time of this work was the same with Cu-CDs, which detected P-NP directly, while the detection limit was lower than it. The comparison of the table showed that the F-PDA-MIS in this experiment had a relatively narrow linear range, but a faster response time and lower detection limit, which could achieve fast and efficient detection of P-NP in drinking water.

Detection of P-NP in drinking water

The final purpose of preparation of F-PDA-MIS was to apply it to the detection of actual samples; the drinking water that people drink every day was taken as the research object;

mineral water was bought from supermarket in the university as one of the drinking water samples; another sample was the drinking water of the boiling water room in the university dormitory. The two groups of samples were divided into six groups, which three of the six groups were added different concentrations of P-NP; another three groups were without P-NP; each set of samples were detected for three times and then took the average value to confirm the accuracy and preciseness of the detective experiment. The corresponding results are listed in Table 1, the recovery rates of mineral water and boiling water were 98.6–106% and 98.0–104% with RSD of 2.7–3.4% and 2.6–3.5% respectively. Compared with the results of samples added P-NP to that without P-NP, the concentration of P-NP could be detected by both two groups; in other words, the F-PDA-MIS which synthesized this experiment could analyze the concentration of P-NP effectively. To further verify the accuracy of F-PDA-MIS in

Table 1 Results of P-NP determination in drinking water samples

	Sample number	Determined (nM)	Added (nM)	Found (nM)	Recover (%)	RSD (% , n = 3)
Mineral water	1	<LOD	500	490	98.0	2.8
		24.6	800	819	102	3.4
	2	25.0	500	514	103	2.9
		<LOD	800	799	100	2.7
	3	24.9	500	519	104	3.1
		24.3	800	822	103	2.9
Boiling water	1	25.1	500	516	103	3.2
		<LOD	800	789	98.6	2.7
	2	31.2	500	531	106	3.3
		29.0	800	831	104	2.9
	3	29.0	500	532	106	2.6
		33.9	800	837	105	3.5

Table 2 Comparisons of P-NP determination results in drinking water samples by fluorescence analysis method and HPLC–UV method

Samples	Added (nM)	F-PDA@MIS			HPLC–UV		
		Found (nM)	Recover (%)	RSD (% , n = 3)	Found (nM)	Recover (%)	RSD (% , n = 3)
Mineral water	800	819	102	3.4	813	102	2.6
		799	100	2.7	814	102	2.5
		822	103	2.9	813	102	2.7
Boiling water	800	789	98.6	2.7	831	104	2.9
		831	104	2.9	833	104	2.7
		837	105	3.5	836	107	2.6

detecting P-NP, the standard recovery experiments of P-NP in mineral water and boiling water via HPLC–UV were conducted for the comparison. The HPLC–UV results are displayed in Figure S9, and the comparison results are listed in Table 2; the found concentrations of P-NP in mineral water and boiling water were 13.4 nM and 33.4 nM, which were basically in line with the results found by fluorescence analysis method. The comparison experiment convincingly proved that the fluorescence analysis method could detect P-NP accurately and rapidly.

In summary, based on the excellent biocompatibility of F-PDA, the research of this experiment had laid a good foundation for its application in the field of biological monitoring and detection. However, there are still areas for improvement in the experiment. For example, the selectivity of F-PDA-MIS needs to be improved. Because F-PDA directly participates in the reaction, it is inevitable that part of F-PDA will be exposed outside the imprinting layer, which will speed up the response time and it will also reduce the selectivity of F-PDA-MIS. This is where we need to improve in the following experiment, and it also provides a guiding direction for the next experiment.

Conclusion

In this work, a homogeneous and stable F-MIS has been successfully synthesized for selective recognition of P-NP, in which F-PDA was firstly put forward as both fluorescence monomer and functional monomer. In comparison of conventional QDs-based and dyes-based fluorescent molecularly imprinted sensor, F-MIS could realize ultra-fast detection of P-NP with low detection limit. The selective detection results showed that F-MIS exhibited highly selectivity among complex isomers in water samples. Then, the anti-interference experiment proved the superiority of F-MIS again. The final results of the determination of P-NP in drinking water samples verified the practicality of F-MIS. To sum up, F-PDA as a highly effective fluorescence functional monomer could quickly complete the electron transfer between F-PDA and P-NP and realize the fluorescence

quenching of F-PDA by P-NP. The application of F-PDA in molecularly imprinted fluorescent sensors showed a bright prospect for ultra-trace analysis and detection.

Supplementary Information The online version contains supplementary material available at <https://doi.org/10.1007/s00604-021-05106-3>.

Funding This work was supported by the National Natural Science Foundation of China (Nos. 21808089, 51803080), China Postdoctoral Science Foundation (No. 2019M661750, 2019T120400), Natural Science Foundation of Jiangsu Province (No. BK20190245), Major projects of education department of Jiangsu province (No. 17KJA530003), and Programs of Senior Talent Foundation of Jiangsu University (No. 15JDG024).

Declarations

Conflict of interest The authors declare no conflict of interest.

References

- Han L, Liu SG, Liang JY, Ju YJ, Li NB, Luo HQ (2019) pH-mediated reversible fluorescence nanoswitch based on inner filter effect induced fluorescence quenching for selective and visual detection of 4-nitrophenol. *J Hazard Mater* 362:45–52. <https://doi.org/10.1016/j.jhazmat.2018.09.025>
- Hu YP, Gao ZJ (2020) Sewage sludge in microwave oven: a sustainable synthetic approach toward carbon dots for fluorescent sensing of para-Nitrophenol. *J Hazard Mater* 382:121048. <https://doi.org/10.1016/j.jhazmat.2019.121048> ((1-7))
- Qiu N, Liu Y, Xiang M, Lu XM, Yang Q, Guo R (2018) A facile and stable colorimetric sensor based on three-dimensional graphene/mesoporous Fe₃O₄ nanohybrid for highly sensitive and selective detection of p-nitrophenol. *Sensors Actuators B Chem* 266:86–94. <https://doi.org/10.1016/j.snb.2018.03.059>
- Bo LL, Quan X, Chen S, Zhao HM, Zhao YZ (2006) Degradation of p-nitrophenol in aqueous solution by microwave assisted oxidation process through a granular activated carbon fixed bed. *Water Res* 40:3061–3068. <https://doi.org/10.1016/j.watres.2006.06.030>
- Zhai HY, Xiao WL, Li Y, Li RZ, Liu HJ, Yu LP (2020) Sensitive and selective determination of 4-nitrophenol in water and food using modified polyethyleneimine-capped carbon dots. *J Chin Chem Soc* 67:1230–1238. <https://doi.org/10.1002/jccs.201900494>
- Wei Y, Kong LT, Yang R, Wang L, Liu JH, Huang XJ (2011) Single-walled carbon nanotube/pyrenecyclodextrin nanohybrids

- for ultrahighly sensitive and selective detection of p-nitrophenol. *Langmuir* 27:10295–10301. <https://doi.org/10.1021/la201691c>
- Le XD, Dong ZP, Liu YS, Jin ZC, Huy TD, Le M, Ma JT (2014) Palladium nanoparticles immobilized on core-shell magnetic fibers as a highly efficient and recyclable heterogeneous catalyst for the reduction of 4-nitrophenol and Suzuki coupling reactions. *J Mater Chem A* 2:19696–19706. <https://doi.org/10.1039/C4TA04919E>
 - Wang ML, Jiang TT, Lu Y, Liu HJ, Chen Y (2013) Gold nanoparticles immobilized in hyperbranched polyethylenimine modified polyacrylonitrile fiber as highly efficient and recyclable heterogeneous catalysts for the reduction of 4-nitrophenol. *J Mater Chem A* 1:5923–5933. <https://doi.org/10.1039/C3TA10293A>
 - Uzer A, Ercag E, Apak R (2004) Selective spectrophotometric determination of trinitrotoluene, trinitrophenol, dinitrophenol and mononitrophenol. *Anal Chim Acta* 505:83–93. [https://doi.org/10.1016/S0003-2670\(03\)00674-3](https://doi.org/10.1016/S0003-2670(03)00674-3)
 - Colades JJ, de Luna MDG, Segondes MFN, Huang CP (2019) Electrochemical in-situ hydrogen peroxide generation in a packed-bed reactor for Fenton oxidation of p-nitrophenol in aqueous solution. *Process Saf Environ Prot* 123:161–168. <https://doi.org/10.1016/j.psep.2018.10.014>
 - Zhang JJ, Cui SQ, Ding YP, Yang XX, Guo K, Zhao JT (2018) Two-dimensional mesoporous ZnCo₂O₄ nanosheets as a novel electrocatalyst for detection of o-nitrophenol and p-nitrophenol. *Biosens Bioelectron* 112:177–185. <https://doi.org/10.1016/j.bios.2018.03.021>
 - Yamauchi Y, Ido M, Ohta M, Maeda H (2004) High performance liquid chromatography with an electrochemical detector in the cathodic mode as a tool for the determination of p-nitrophenol and assay of acid phosphatase in urine samples. *Chem Pharm Bull* 52:552–555. <https://doi.org/10.1248/cpb.52.552>
 - Skog KM, Xiong FLZ, Kawashima H, Doyle E, Soto R, Gentner DR (2019) Compact, automated, inexpensive, and field-deployable vacuum-outlet gas chromatograph for trace-concentration gas-phase organic compounds. *Anal Chem* 91:1318–1327. <https://doi.org/10.1021/acs.analchem.8b03095>
 - Shirani MP, Rezaei B, Ensaifi AA, Ramezani M (2021) Development of an eco-friendly fluorescence nanosensor based on molecularly imprinted polymer on silica-carbon quantum dot for the rapid indoxacarb detection. *Food Chem* 339:127920. <https://doi.org/10.1016/j.foodchem.2020.127920> ((1-7))
 - Huang SY, Guo ML, Tan JA, Geng YY, Wu JY, Tang YW, Su CC, Lin CC, Liang Y (2018) Novel fluorescence sensor based on all-inorganic perovskite quantum dots coated with molecularly imprinted polymers for highly selective and sensitive detection of omethoate. *ACS Appl Mater Interfaces* 10:39056–39063. <https://doi.org/10.1021/acsami.8b14472>
 - Wang T, Wei X, Zong Y, Zhang S, Guan W (2020) An efficient and stable fluorescent sensor based on APTES-functionalized CsPbBr₃ perovskite quantum dots for ultrasensitive tetracycline detection in ethanol. *J Mater Chem C* 8:12196–12203. <https://doi.org/10.1039/D0TC02852E>
 - Yang Q, Li JH, Wang XY, Xiong H, Chen LX (2019) Ternary emission of a blue-, green-, and red-based molecular imprinting fluorescence sensor for the multiplexed and visual detection of bovine hemoglobin. *Anal Chem* 91:6561–6568. <https://doi.org/10.1021/acs.analchem.9b00082>
 - Wang JX, Cheng RJ, Wang YY, Sun L, Chen L, Dai XH, Pan JM, Pan GQ, Yan YS (2018) Surface-imprinted fluorescence microspheres as ultrasensitive sensor for rapid and effective detection of tetracycline in real biological samples. *Sensors Actuators B Chem* 263:533–542. <https://doi.org/10.1016/j.snb.2018.02.150>
 - Wang Z, Xu C, Lu YX, Wei GY, Ye G, Sun TX, Chen J (2018) Microplasma electrochemistry controlled rapid preparation of fluorescent polydopamine nanoparticles and their application in uranium detection. *Chem Eng J* 344:480–486. <https://doi.org/10.1016/j.cej.2018.03.096>
 - Chen MH, Wen Q, Gu FL, Gao JW, Zhang CC, Wang QM (2018) Mussel chemistry assembly of a novel biosensing nanoplatform based on polydopamine fluorescent dot and its photophysical features. *Chem Eng J* 342:331–338. <https://doi.org/10.1016/j.cej.2018.02.099>
 - Nam H, Kim B, Ko M, Jin M, Kim JM, Jung DY (2012) A new mussel-inspired polydopamine sensitizer for dye-sensitized solar cells: controlled synthesis and charge transfer. *Chem Eur J* 18:14000–14007. <https://doi.org/10.1002/chem.201202283>
 - Cao Y, Zhang X, Tao L, Li K, Xue Z, Feng L, Wei Y (2013) Mussel-inspired chemistry and Michael addition reaction for efficient oil/water separation. *ACS Appl Mater Interfaces* 5:4438–4442. <https://doi.org/10.1021/am4008598>
 - Cheng C, Nie S, Li S, Peng H, Yang H, Ma L, Sun S, Zhao C (2013) Biopolymer functionalized reduced graphene oxide with enhanced biocompatibility via mussel inspired coatings/anchors. *J Mater Chem B* 1:265–275. <https://doi.org/10.1039/C2TB00025C>
 - Lee Y, Lee H, Kim YB, Kim J, Hyeon T, Park H, Messersmith PB, Park TG (2008) Bioinspired surface immobilization of hyaluronic acid on monodisperse magnetite nanocrystals for targeted cancer imaging. *Adv Mater* 20:4154–4157. <https://doi.org/10.1002/adma.200800756>
 - Ma Y-R, Niu H-Y, Zhang X-L, Cai Y-Q (2011) Colorimetric detection of copper ions in tap water during the synthesis of silver/dopamine nanoparticles. *Chem Commun* 47:12643–12645. <https://doi.org/10.1039/C1CC15048K>
 - Zhang L, Wu J, Wang Y, Long Y, Zhao N, Xu J (2012) Combination of bioinspiration: a general route to superhydrophobic particles. *J Am Chem Soc* 134:9879–9881. <https://doi.org/10.1021/ja303037j>
 - Zhang X, Wang S, Xu L, Feng L, Ji Y, Tao L, Li S, Wei Y (2012) Biocompatible polydopamine fluorescent organic nanoparticles: facile preparation and cell imaging. *Nanoscale* 4:5581–5584. <https://doi.org/10.1039/C2NR31281F>
 - Liu XS, Cao JM, Li H, Li JY, Jin Q, Ren KF, Ji J (2013) Mussel-inspired polydopamine: a biocompatible and ultrastable coating for nanoparticles in vivo. *ACS Nano* 7:9384–9395. <https://doi.org/10.1021/nn404117j>
 - Chien HW, Kuo WH, Wang MJ, Tsai SW, Tsai WB (2012) Tunable micropatterned substrates based on poly(dopamine) deposition via microcontact printing. *Langmuir* 28:5775–5782. <https://doi.org/10.1021/la300147p>
 - Fu YC, Li PH, Xie QJ, Xu XH, Lei LH, Chen C, Zou C, Deng WF, Yao SZ (2009) One-pot preparation of polymer-enzyme-metallic nanoparticle composite films for high-performance biosensing of glucose and galactose. *Adv Func Mater* 19:1784–1791. <https://doi.org/10.1002/adfm.200801576>
 - Wan Q, Wang K, Du HL, Huang HY, Liu MY, Deng FJ, Dai YF, Zhang XY, Wei Y (2015) A rather facile strategy for the fabrication of PEGylated AIE nanoprobcs. *Polym Chem* 6:5288–5294. <https://doi.org/10.1039/C5PY00735F>
 - Ma L, Qin H, Cheng C, Xia Y, He C, Nie CX, Wang LR, Zhao CS (2014) Mussel-inspired self-coating at macro-interface with improved biocompatibility and bioactivity via dopamine grafted heparin-like polymers and heparin. *J Mater Chem B* 2:363–375. <https://doi.org/10.1039/C3TB21388A>
 - Cheng C, Sun SD, Zhao CS (2014) Progress in heparin and heparin-like/mimicking polymer-functionalized biomedical membranes. *J Mater Chem B* 2:7649–7672. <https://doi.org/10.1039/C4TB01390E>
 - Liu MY, Ji JZ, Zhang XY, Zhang XQ, Yang B, Deng FJ, Li Z, Wang K, Yang Y, Wei Y (2015) Self-polymerization of dopamine and polyethylenimine: novel fluorescent organic nanoprobcs for

- biological imaging applications. *J Mater Chem B* 3:3476–3482. <https://doi.org/10.1039/C4TB02067G>
35. Wang R, Yu B, Jiang XS, Yin J (2012) Understanding the host-guest interaction between responsive core-crosslinked hybrid nanoparticles of hyperbranched poly(ether amine) and dyes: the selective adsorption and smart separation of dyes in water. *Adv Func Mater* 22:2606–2616. <https://doi.org/10.1002/adfm.201102902>
36. Liu XQ, Zhou ZP, Wang T, Deng PY, Yan YS (2020) Visual monitoring of trace water in organic solvents based on ecofriendly b/r-CDs ratiometric fluorescence test paper. *Talanta* 216:120958. <https://doi.org/10.1016/j.talanta.2020.120958> (1-7)
37. Xiao N, Liu SG, Mo S, Li N, Ju YJ, Ling Y, Li NB, Luo HQ (2018) Highly selective detection of p-nitrophenol using fluorescence assay based on boron, nitrogen co-doped carbon dots. *Talanta* 184:184–192. <https://doi.org/10.1016/j.talanta.2018.02.114>
38. Sun J, Zhao JH, Wang L, Li HW, Yang F, Yang XR (2018) Inner filter effect-based sensor for horseradish peroxidase and its application to fluorescence immunoassay. *ACS Sens* 3:183–190. <https://doi.org/10.1021/acssensors.7b00830>
39. Ma YS, Cen Y, Sohail M, Xu GH, Wei FD, Shi ML, Xu XM, Song YY, Ma YJ, Hu Q (2017) A ratiometric fluorescence universal platform based on N, Cu Codoped carbon dots to detect metabolites participating in H₂O₂-generation reactions. *ACS Appl Mater Interfaces* 9:33011–33019. <https://doi.org/10.1021/acsami.7b10548>
40. Foroughirad S, Haddadi-Asl V, Khosravi A, Salami-Kalajahi M (2021) Magnetic halloysite-based molecularly imprinted polymer for specific recognition of sunset yellow in dyes mixture. *Polym Adv Technol* 32:803–814. <https://doi.org/10.1002/pat.5132>

Publisher's note Springer Nature remains neutral with regard to jurisdictional claims in published maps and institutional affiliations.